Magnetic anisotropy and spin-disordered ground state in the triangular-lattice antiferromagnet $K_2CsYb(PO_4)_2$

Xin-An Tong,[1,*] Yingqi Chen,[1,*] Zhongtuo Fu,[1] Shuaiwei Li,[1] Tianci Gao,[1] Hong Du,[2] Shuhan Zheng,[1] Yongjun Zhang,[1] Yunlong Xie,[1] Meifeng Liu,[1] Ruidan Zhong,[2] Jun-Ming Liu,[3,4,5] Zhen Ma,[1,†] Wei Wang,[5,6,‡] and Jinsheng Wen[3,4,5,§]

[1]*Hubei Key Laboratory of Photoelectric Materials and Devices, School of Materials Science and Engineering, Hubei Normal University, Huangshi 435002, China*

[2]*Tsung-Dao Lee Institute & School of Physics and Astronomy, Shanghai Jiao Tong University, Shanghai 200240, China*

[3]*National Laboratory of Solid State Microstructures and Department of Physics, Nanjing University, Nanjing 210093, China*

[4]*Collaborative Innovation Center of Advanced Microstructures, Nanjing University, Nanjing 210093, China*

[5]*Jiangsu Physical Science Research Center, Nanjing University, Nanjing 210093, China*

[6]*School of Science, Nanjing University of Posts and Telecommunications, Nanjing 210023, China*

(Received 19 September 2025; revised 4 December 2025; accepted 9 January 2026; published 30 January 2026)

Triangular-lattice compounds serve as a prototypical example of geometrically frustrated systems and can host a variety of quantum states, among which quantum spin liquids (QSLs) are particularly intriguing. However, structural disorder is often present in real QSL candidates and it may drive the system into a spin-glass state. Here, we have successfully grown the single crystals of a new triangular-lattice rare-earth compound $K_2CsYb(PO_4)_2$. X-ray diffractions confirm high phase purity with no detectable structural disorder. The dc magnetic susceptibility measurements reveal dominant magnetic anisotropy, with a stronger response in the *ab* plane than along the *c* axis. Notably, no phase transition or spin freezing is observed, as further corroborated by ac susceptibility measurements down to 400 mK. Moreover, specific heat measurements down to 50 mK show no hint of long-range magnetic order either, but only an anomaly that can be well fitted by a two-level Schottky function due to the splitting of the Kramers doublet ground state. Collectively, these findings point to a spin disordered ground state consistent with QSL behaviors. To gain deeper insight into the underlying physics, first-principles calculations based on density functional theory are carried out, suggesting a strong spin-orbit entangled ground state characterized by an effective spin $J_{\text{eff}} = 1/2$. Our work establishes $K_2CsYb(PO_4)_2$ as a pristine platform for exploring novel quantum states in a perfect triangular-lattice system.

DOI: 10.1103/jzd6-5354

I. INTRODUCTION

Geometrical frustration provides a fundamental mechanism for introducing quantum fluctuations into a magnetic system, which can give rise to a variety of quantum states [1–3]. Especially in triangular-lattice rare-earth compounds, the spin-orbit entangled nature of $4f$ electrons often results in anisotropic spin interactions that further enhance these fluctuations and may bring a quantum disordered state known as quantum spin liquids (QSLs) [4–7]. This novel state remains a topical issue in modern condensed matter physics due to the relevance to high-temperature superconductivity [8,9] and potential applications in topological quantum computation [10,11]. To gain deeper insight into the QSL physics, the search for real QSL materials has become an ongoing task since Anderson proposed the prototype of the resonating valence bond model [12–14].

Among the triangular-lattice rare-earth materials, ytterbium-based compounds stand out as the promising QSL candidates [4,15–17], since their small effective spin $J_{\text{eff}} = 1/2$ favors a dynamically fluctuating ground state [4,5,15]. A notable example is the triangular-lattice antiferromagnet $YbMgGaO_4$, which has garnered substantial attention in recent years due to the possible realization of a gapless QSL [4,18–20]. This claim is supported by multiple experimental observations, including the power-law temperature dependence of magnetic specific heat [18,20], persistent spin dynamics at subkelvin temperatures evidenced by muon spin relaxation (μSR) spectra [21,22], and spin excitation continuum captured in neutron scattering spectra [19,20]. However, further investigations of thermal conductivity fail to probe the itinerant spinons expected in a QSL [23]. Instead, the ac magnetic susceptibility measurements directly reveal a spin-glass transition near 0.1 K [24], casting doubt on the initial scenario of a QSL. Regarding the discrepancy among these findings, a vigorous debate is ongoing. The crux of the matter lies in whether the observed spin-liquid-like behaviors originate from intrinsic quantum fluctuations or from structural disorder caused by Mg^{2+}/Ga^{3+} site mixing [24–28]. Such a problem is actually ubiquitous in other QSL candidates [13,14,29,30]. For

*These authors contributed equally to this work.
†Contact author: zma@hbnu.edu.cn
‡Contact author: wwang@njupt.edu.cn
§Contact author: jwen@nju.edu.cn

 ©2026 American Physical Society

instance in the well-known herbertsmithite $ZnCu_3(OH)_6Cl_2$, antisite disorder between Cu^{2+} and Zn^{2+} ions is significant and it may contribute to the low-energy magnetic excitations [31,32], complicating the interpretation of its intrinsic ground state upon an ideal kagome framework [33–35].

Motivated by the disorder problem in real QSL candidates, the new class of ytterbium-based compounds $AYbCh_2$ (A = alkali metal, Ch = chalcogen) have emerged as a promising alternative [36–41]. The significant difference in ionic radii between alkali-metal ions and Yb^{3+} effectively preclude structural disorder in these materials [15]. Nevertheless, considering the challenge in preparing high-quality and large-sized single crystals, especially for the oxygen- and sulfur-containing members within this category [7,15,37], further exploration of new ytterbium-based triangular-lattice compounds that are both free from disorder and accessible in the single-crystals form has become a vital step toward well understanding the novel quantum states inherent in geometrically frustrated systems.

In this work, we report the successful synthesis and comprehensive characterizations of a new triangular-lattice compound, $K_2CsYb(PO_4)_2$. X-ray diffraction (XRD) reveals the high phase purity and a disorder-free triangular framework. Magnetic anisotropy is evident from the dc magnetic susceptibility results, where larger susceptibility in the ab plane (||) than that along the c axis ($\perp$) is characteristic of easy-plane type. A fit to the low-temperature data yields the Curie-Weiss temperature $\Theta_{||} = -0.03$ K and $\Theta_{\perp} = -0.71$ K for these two directions, respectively, indicating the dominant antiferromagnetic interactions. The extracted Landé factors $g_{||} = 3.00$ and $g_{\perp} = 1.99$ agree well with that of $g_{||} = 2.85$ and $g_{\perp} = 1.83$ derived from the isothermal field dependent magnetization data. Remarkably, no phase transition or spin freezing is detected down to 1.8 K, as confirmed by the ac susceptibility extending to 400 mK. Ultralow-temperature specific heat measurements down to 50 mK reveal no λ-shaped peak indicative of a phase transition, but show a Schottky anomaly that is well described by a two-level system. Further first-principles calculations based on density functional theory establish a spin-orbit entangled ground state with an effective spin $J_{\text{eff}} = 1/2$, suggesting the intriguing quantum magnetism in this new compound.

II. EXPERIMENTAL AND COMPUTATIONAL METHODS

Polycrystalline samples of $K_2CsYb(PO_4)_2$ were synthesized via the conventional solid-state reaction method. The raw materials K_2CO_3 (99.99%), Cs_2CO_3 (99.99%), Yb_2O_3 (99.99%), and $(NH_4)_2HPO_4$ (99.99%) were dried before weighing and were thoroughly ground in a stoichiometric proportion. Then the well-mixed precursors were loaded into an alumina crucible and heated at 800 °C in air for 96 h, with an intermediate grinding to ensure phase purity. High-quality single crystals were grown by the high-temperature flux method through spontaneous crystallization, so the obtained crystals exhibit a mirrorlike cleaved surface with the largest edge up to 1 cm, as shown in the left inset of Fig. 1(d).

XRD data of polycrystalline samples were collected at room temperature in an x-ray diffractometer (SmartLab SE, Rigaku) using the Cu-K_α edge with a wavelength of 1.54 Å,

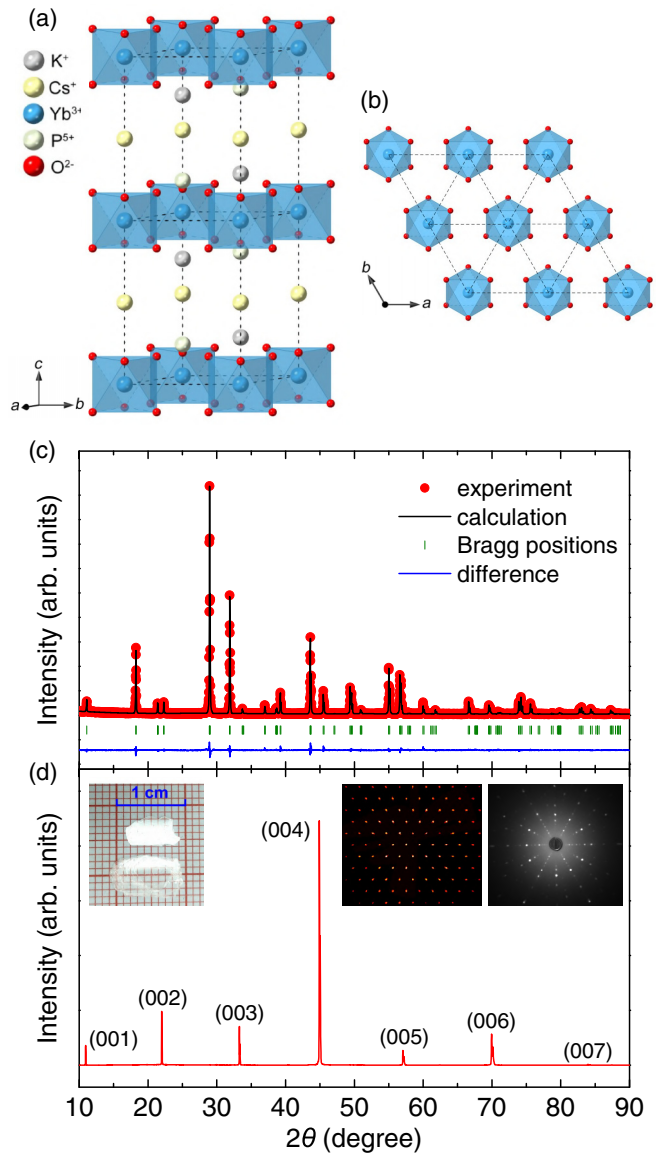


FIG. 1. (a) Schematic crystal structure of $K_2CsYb(PO_4)_2$. (b) Top view of the magnetic triangular layer consisting of YbO_6 octahedra. (c) Rietveld refinement results of room-temperature XRD data for $K_2CsYb(PO_4)_2$. Red circles, black solid line, and green ticks indicate the measured data points, calculated results upon Rietveld refinements, and Bragg peak positions, respectively. Blue solid line represents the difference between the experiments and calculations. (d) XRD data taken on the (00L) crystal surface. Left, middle, and right insets show a photograph of transparent $K_2CsYb(PO_4)_2$ single crystals, the single-crystal XRD pattern of the (HK0) reflection plane, and the x-ray Laue pattern of the (00L) plane, respectively.

while the cleaved surface of a single crystal was identified as the (00L) plane by another x-ray diffractometer (D8 Advance Eco, Bruker) with the same setting parameters. Rietveld refinements on the XRD data were performed by GSAS software. Single-crystal XRD data were collected at room temperature in an x-ray diffractometer (XtaLAB Synergy-R, Rigaku) using Mo-K_α radiation with a wavelength of 0.71 Å. The observed reflections were indexed and integrated using the data reduction program CRYSALISPRO. An x-ray

backscattering Laue (Photonic Science) pattern was taken with the beam perpendicular to the cleavage plane. The dc magnetic susceptibility was measured on a piece of single crystal with the field applied parallel and perpendicular to the *ab* plane, respectively, over the temperature range of 1.8–350 K in a Quantum Design physical property measurement system (PPMS, Dynacool) equipped with a vibrating sample magnetometer option. The ac susceptibility data were obtained in a Quantum Design magnetic property measurement system with a He3 insert for temperature ranging from 0.4 to 3 K and for driving frequencies from 50 to 1000 Hz. Ultralow-temperature specific heat was measured by the relaxation method in a PPMS Dynacool equipped with a dilution refrigerator, which allows for measurements down to 50 mK. The optical diffuse reflectance spectra were obtained at room temperature in a UV-Vis-NIR spectrometer (Cary 5000, Agilent) with wavelengths from 200 to 2000 nm.

The first-principles calculations were performed using the Vienna *Ab initio* Simulation Package (VASP) [42] based on density functional theory. The projector augmented wave method was employed to describe the effect of core electrons [43]. The exchange-correlation functional was treated within the generalized gradient approximation of Perdew-Burke-Ernzerhof [44]. The energy cutoff for the plane-wave basis set was set to 520 eV, and a Γ-centered $9 \times 9 \times 4$ Monkhorst-Pack k-point mesh was used for the Brillouin zone sampling. The experimentally determined crystal structure was adopted in our calculations.

III. RESULTS

A. Crystal structure and x-ray diffraction

Figures 1(a) and 1(b) illustrate the schematics of the crystal structure and a magnetic triangular layer of $K_2CsYb(PO_4)_2$, respectively. It crystallizes in the space group $P\bar{3}m1$, isostructural to our recently synthesized rare-earth compounds $Rb_3Yb(VO_4)_2$ and $Cs_3Yb(VO_4)_2$ [17]. The magnetic layers are composed of edge-sharing YbO_6 octahedra and are directly stacked with an *AAA* sequence along the c axis, in contrast with the *ABC* arrangement commonly observed in ytterbium-based QSL candidates, such as $YbMgGaO_4$ and the $AYbCh_2$ family [15,18]. Nonmagnetic ions of alkali metals fully occupy the interlayer sites, effectively suppressing the magnetic exchange interactions along the c axis.

We firstly collected the XRD data at room temperature for polycrystalline samples of $K_2CsYb(PO_4)_2$, and the results along with the Rietveld refinements are shown in Fig. 1(c). There is an excellent agreement between the experimental and calculated results, with no impurity phase detected in the sample. The refinements yield the lattice parameters $a = b = 5.61406(12)$ Å, $c = 7.97402(24)$ Å, and $\alpha = \beta = 90°$, $\gamma = 120°$. From this result, we calculate the ratio of interlayer-to-intralayer distance ($d_{\text{inter}}/d_{\text{intra}}$) for the nearest-neighbor Yb^{3+} ions to be 1.42. This value is a bit larger than that of 1.32 determined in another QSL candidate $Na_2BaCo(PO_4)_2$ [45], which also features *AAA*-stacked triangular magnetic layers, suggesting the enhanced two-dimensional magnetic isolation in $K_2CsYb(PO_4)_2$. The final refinement parameters are $R_p \approx 6.56\%$, $R_{wp} \approx 8.82\%$, and $\chi^2 \approx 2.57$. These low values demonstrate the goodness of fitting and high phase purity of our synthesized samples. On the other hand, single-crystal XRD diffraction was also performed to confirm the structure, as shown in the middle inset of Fig. 1(d). The comparison of main structural parameters yielded from both powder and single-crystal diffractions are summarized in Table I, exhibiting no significant difference between the two datasets. It is worth noting that the occupancies for different types of ions are all 1, confirming the structurally disorder-free nature for this compound. Additionally, we also characterized the cleaved surface of the single crystals using both an x-ray diffractemeter and an x-ray backscattering Laue diffractometer. As shown in Fig. 1(d), all the observed peaks are sharp and can be indexed as (00L) reflections, indicating the high quality of the measured single crystal. This is further confirmed by the Laue pattern shown in the right inset of Fig. 1(d). It exhibits clear and bright spots with a sixfold symmetry, characteristic of a triangular framework.

TABLE I. Refined structural parameters upon both powder and single-crystal XRD data collected at room temperature for $K_2CsYb(PO_4)_2$.

Sample type	Atom	Site	x	y	z	Occ.	U_{iso} (Å^2)
Powder	K	2d	0.3333	0.6667	0.2621	1	0.016
	Cs	1b	0	0	0.5	1	0.016
	Yb	1a	0	0	0	1	0.025
	P	2d	0.3333	0.6667	0.7786	1	0.007
	O(1)	6i	0.1985	0.8015	0.8246	1	0.019
	O(2)	2d	0.3333	0.6667	0.5486	1	0.023
Single crystal	K	2d	0.3333	0.6667	0.2504	1	0.019
	Cs	1b	0	0	0.5	1	0.019
	Yb	1a	0	0	0	1	0.008
	P	2d	0.3333	0.6667	0.7723	1	0.007
	O(1)	6i	0.1846	0.8155	0.8398	1	0.020
	O(2)	2d	0.3333	0.6667	0.5843	1	0.024

B. Magnetic susceptibility

Figure 2(a) depicts the temperature dependence of dc magnetic susceptibility (χ) measured with the fields applied both parallel and perpendicular to the *ab* plane. As temperature decreases from 350 to 1.8 K, the susceptibility increases gradually along both directions, but more rapidly within the *ab* plane than along the c axis, suggesting pronounced easy-plane magnetic anisotropy. Notably, no evidence of long-range magnetic transition is observed in the measured temperature range. Furthermore, the absence of bifurcation between zero-field-cooling (ZFC) and field-cooling (FC) data excludes a spin-glass state. Figure 2(b) shows the corresponding inverse susceptibility data. At high temperatures, it exhibits a linear behavior and can be well described by the Curie-Weiss law $\chi = C/(T - \Theta)$ above 150 K, where C and Θ denote Curie-Weiss constant and Curie-Weiss temperature, respectively. From this fit, we obtain $\Theta_{||} = -82.39$ K and $\Theta_{\perp} = -47.85$ K, with the effective moments $\mu_{\text{eff}} = 4.17$ and $4.35\mu_B$ for these two directions, respectively. These values of the effective moments are close to the expected $4.54\mu_B$ for a free Yb^{3+} ion in a trivial paramagnet [46]. We emphasize that the high-temperature fitting just reflects the thermally

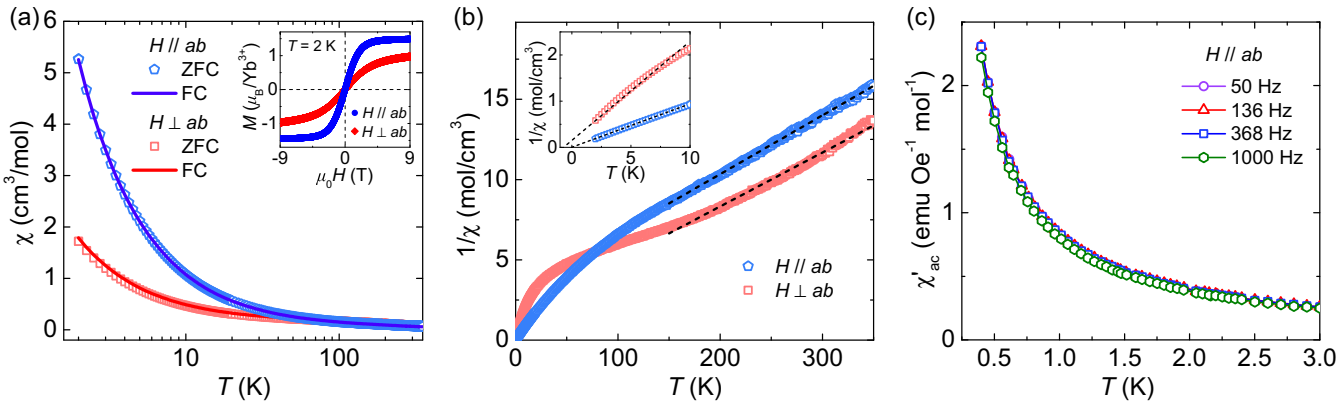


FIG. 2. (a) Temperature dependence of dc magnetic susceptibility (χ) for $K_2CsYb(PO_4)_2$ single crystals measured along two distinct directions at a field of 0.1 T. The measurements were performed both at zero-field-cooling (ZFC) and field-cooling (FC) conditions. These data are corrected by subtracting the Van Vleck paramagnetic susceptibility (χ_{VV}) extracted from Fig. 3. The inset shows complete magnetic loops along two directions at 2 K. (b) Temperature dependence of inverse dc susceptibility obtained from the ZFC data shown in (a). The inset shows the zoom-in view of low-temperature data. The dashed lines are the fits to high- and low-temperature data with the Curie-Weiss law, as described in the main text. (c) Temperature dependence of the real part of ac susceptibility (χ'_{ac}) with different driving frequencies. In this measurement, an excitation field of 0.5 Oe was applied in the *ab* plane.

populated state, where spin correlations are suppressed by thermal fluctuations. To reveal the intrinsic physics associated with the ground state, we perform such a fitting to low-temperature data, as shown in the inset of Fig. 2(b). It gives rise to $\Theta_{||} = -0.03$ K and $\Theta_{\perp} = -0.71$ K, with $\mu_{\text{eff}} = 2.60$ and $1.72\mu_B$, respectively. The negative sign of Curie-Weiss temperatures suggests dominant antiferromagnetic interactions between Yb^{3+} moments albeit with weak strength, consistent with the absence of hysteresis in the magnetic loops, as shown in the inset of Fig. 2(a). To estimate the superexchange coupling constant J, we adopt the XXZ model to $K_2CsYb(PO_4)_2$, which gives $J = (4J_{\pm} + J_{zz})/3$ [4,47], where $J_{\pm} = -\Theta_{||}/3 = 0.01$ K and $J_{zz} = -2\Theta_{\perp}/3 = 0.47$ K. The resulting J is calculated to be 0.17 K. The reduced effective moments derived from the low-temperature fitting indicate the development of spin correlations. Using $\mu_{\text{eff}} = g\mu_B\sqrt{J_{\text{eff}}(J_{\text{eff}}+1)}$, we further extract Landé factors $g_{||} = 3.00$ and $g_{\perp} = 1.99$ for these two directions, confirming the nature of spin anisotropy in the ground state. These parameters are summarized in Table II. In addition to the dc susceptibility, the spin disordered behavior of $K_2CsYb(PO_4)_2$ is corroborated by ac susceptibility down to the subkelvin temperature of 400 mK. In Fig. 2(c), the real part of ac susceptibility (χ'_{ac}) shows no any anomaly or frequency-dependent peak for the driving frequencies ranging from 50 to 1000 Hz, further ruling out the long-range magnetic order or a spin-glass state.

Figure 3(a) presents the results of isothermal field-dependent magnetization measured in the *ab* plane at various temperatures. At 2 K, the magnetization increases linearly with the applied field increasing to ~1 T, followed by a smooth transition into a fully saturated regime above ~5 T. The initial linear response reflects the uniform magnetization of electron moments aligned by the external field. Beyond 1 T, the magnetization gradually deviates from the linear behavior and is eventually saturated when the field reaches up to 5 T. The subsequent minor increase at higher fields is attributed to the extrinsic contribution of Van Vleck paramagnetic susceptibility (χ_{VV}) [18,24]. A linear fit to the high-field data yields $\chi_{VV} = 7.89\times10^{-3}$ cm^3/mol and the saturated moment $M_{\text{sat}} = 1.39\mu_B/Yb^{3+}$ within the *ab* plane. For magnetization along the *c* axis, the behavior is qualitatively similar but requires a higher field of ~8 T to fully polarize all the magnetic moments, as shown in Fig. 3(b). The fitting gives $\chi_{VV} = 1.58\times10^{-2}$ cm^3/mol and $M_{\text{sat}} = 0.84\mu_B/Yb^{3+}$ out of the *ab* plane. These differences in saturation field and saturated moments along two directions further confirm the magnetic anisotropy inferred from the temperature dependence of susceptibility shown in Fig. 2(a). As temperature increases from 2 to 50 K, the magnetization diminishes and the saturation case vanishes due to the thermal population of the excited crystalline electric field levels and the suppression of magnetic couplings between Yb^{3+} ions. The magnetization behaviors along both directions can be quantitatively described by the function $M(H) = \chi_{VV}H + gJ_{\text{eff}}N_A\mu_B B_J(H)$ [48], where N_A is Avogadro constant and B_J is Brillouin function. It results in the average Landé factors $g_{||} = 2.85$ and $g_{\perp} = 1.83$ for the in-plane and out-of-plane directions, respectively. They are in good agreement with $g_{||} = 3.00$ and $g_{\perp} = 1.99$ derived from the Curie-Weiss fitting to susceptibility data, both implying the nature of magnetic anisotropy.

TABLE II. Curie-Weiss temperature (Θ) and Landé factor (g) extracted by the Curie-Weiss fitting to low-temperature (LT) and high-temperature (HT) data.

Directions	Θ_{LT} (K)	g_{LT}	Θ_{HT} (K)	g_{HT}
ab plane	−0.03	3.00	−82.39	1.05
c axis	−0.71	1.99	−47.85	1.10

C. Specific heat

To elucidate the ground state of $K_2CsYb(PO_4)_2$, we measured the ultralow-temperature specific heat (C_p) down to 50 mK with the field applied along the *c* axis. Figure 4(a) shows the C_p results at various magnetic fields. For

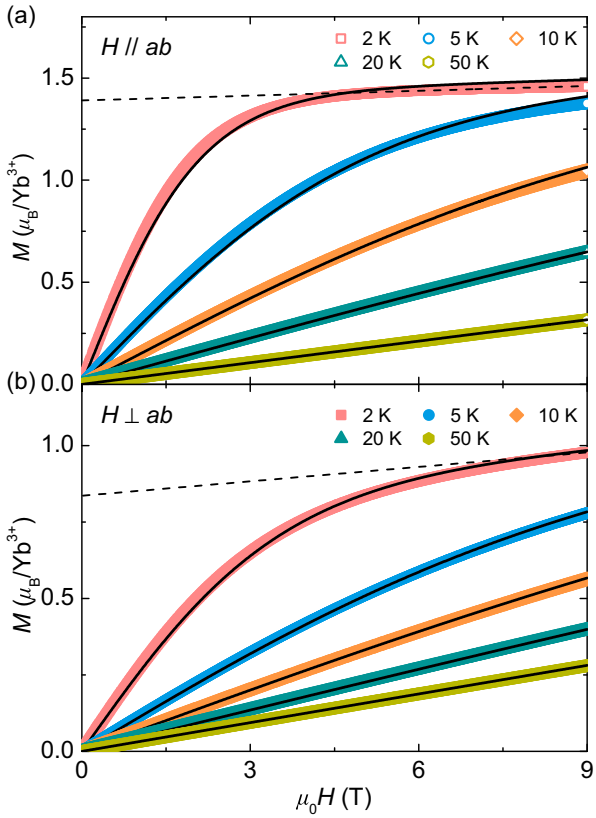


FIG. 3. (a) and (b) Magnetic-field dependence of the magnetization measured at various temperatures with the fields applied parallel and perpendicular to the *ab* plane, respectively. The solid lines are the fits to the data with the combination of Van Vleck contribution and the Brillouin function, as described in the main text. The dashed lines denote the linear fits to the magnetization data in the saturated regime.

comparison, the zero-field specific heat of a nonmagnetic analog $K_2CsLu(PO_4)_2$ is also included, which is well described by a Debye model as $C_p \propto T^3$ and can serve as the pure phonon background of $K_2CsYb(PO_4)_2$. At zero field, $K_2CsYb(PO_4)_2$ exhibits no sharp λ-type peak indicative of a phase transition, but rather an upturn below 200 mK, demonstrating the absence of long-range magnetic order. When a small field of 0.5 T is applied, a broad peak appears near 200 mK and shifts to high temperatures with the increasing fields. The field dependence of this broad peak confirms its magnetic origin. This behavior is reminiscent of the Schottky anomaly arising from the Zeeman splitting of a Kramers doublet ground state, which has been also observed in other ytterbium-based triangular-lattice compounds, such as $KBaYb(BO_3)_2$ [47], $Ba_3Yb(BO_3)_3$ [49], $Ba_6Yb_2Ti_4O_{17}$ [50], etc.

To further obtain the information associated with the magnetic ground state, we extracted the magnetic specific heat (C_m) of $K_2CsYb(PO_4)_2$ by subtracting the phonon contribution using the C_p data of $K_2CsLu(PO_4)_2$, as shown in Fig. 4(b). Indeed, there is no sharp peak observed down to 50 mK, confirming the absence of long-range magnetic order. The overall behavior of C_m at different fields is quite similar with that of C_p except in the high-temperature region, where phonons start

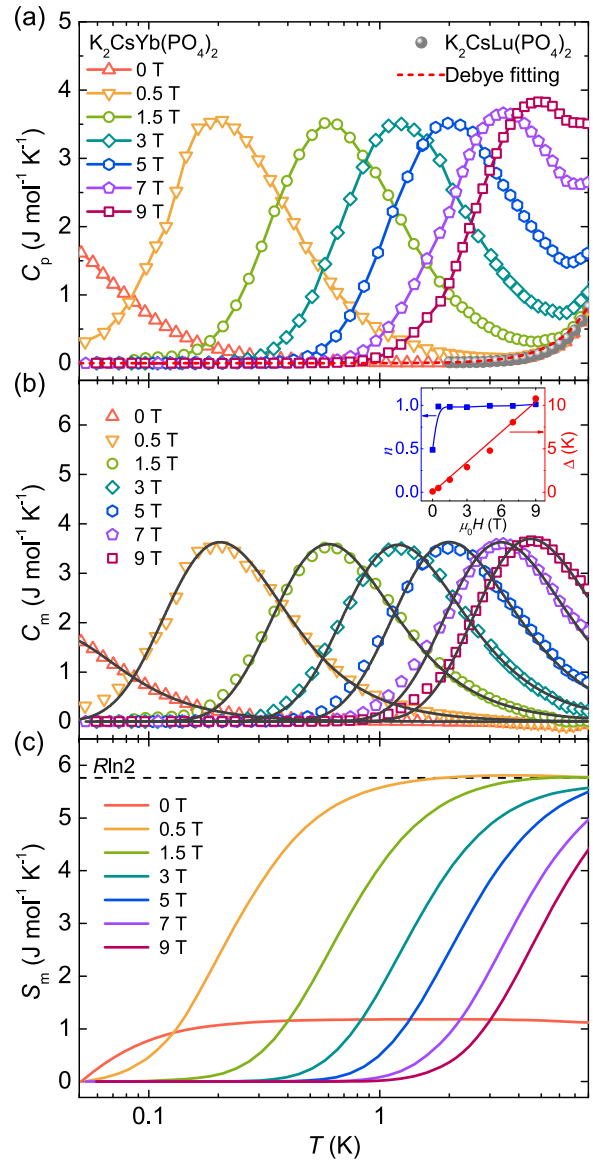


FIG. 4. (a) Ultralow-temperature specific heat (C_p) of $K_2CsYb(PO_4)_2$ single crystals measured with the fields applied along the *c* axis. A nonmagnetic isostructural compound $K_2CsLu(PO_4)_2$ is also measured at zero field, of which the specific heat can be nicely fitted by the Debye model as $C_p \propto T^3$. (b) Magnetic specific heat (C_m) of $K_2CsYb(PO_4)_2$ after subtracting the lattice contribution with the nonmagnetic compound $K_2CsLu(PO_4)_2$. The solid lines represent the fits with a two-level Schottky function, as described in the main text. The inset shows the magnetic-field dependence of the percent of free spins *n* (left vertical axis) and the energy gap Δ (right vertical axis). (c) Temperature dependence of magnetic entropy (S_m) at various fields, which was obtained by integrating C_m/T data. The dashed lines indicate the value of $R\ln 2$, where *R* is the ideal gas constant.

to develop and significantly contribute to the total specific heat above ∼4 K, as shown in Fig. 4(a). The extracted C_m data at these fields are well fitted by a two-level Schottky function [47,48],

$$C_{Sch} = nR\left(\frac{\Delta}{T}\right)^2 \frac{e^{-\Delta/T}}{(1+e^{-\Delta/T})^2}, \quad (1)$$

where n is the molar fraction of free spins, R is the gas constant, and Δ is the Zeeman gap within the Kramers doublet ground state. From this fit, we obtain a series of Δ and n values, which are plotted as a function of $\mu_0 H$ in the inset of Fig. 4(b). As can be seen, n is nearly 0.5 at zero field and rapidly rises to 1 upon application of a small field of 0.5 T, approaching a saturation case. This indicates that half of the spins in the ground state remain correlated and they are all excited to higher energy levels by the applied field, thereby becoming free spins and contributing to the Schottky specific heat. Since all the electrons have been populated, higher fields would not create more free spins. Thus, n remains constant in the process of the fields increasing from 0.5 to 9 T. For the gap Δ, it increases continuously with the applied fields and exhibits a good linear behavior. Using the Zeeman effect relation $\Delta = g\mu_B\mu_0 H$, we obtain the Landé factor $g_\perp = 1.72$. This value is in good agreement with that of 1.99 and 1.83 derived from the above dc susceptibility data. The nearly zero value of Δ at zero field suggests the presence of a doublet ground state in this system.

Figure 4(c) shows the magnetic entropy (S_m) obtained by integrating the C_m/T data at various fields. At zero field, S_m rapidly increases before saturating, reaching a value of 1.17 J mol^{-1} K^{-1} above ~200 mK. This amount represents only 20.3% of Rln2 expected for a $J_{eff} = 1/2$ magnetic ground state. In other words, ~80% magnetic entropy remains unreleased below our measurement limit of 50 mK. This is a nontrivial behavior and is rarely observed in other geometrically frustrated ytterbium-based magnets, where there is hardly any residual entropy at such a low temperature [16,18,24,51]. Once the small external field of 0.5 T is applied on this material, S_m immediately recovers to the full Rln2 entropy around 1 K, characteristic of a two-level magnetic system. As the field continues to increase, the entropy persists, but the critical temperature where it begins to saturate shifts to a higher region, suggesting the field-induced broadening of the spin gap within the Kramers doublet.

D. First-principles calculations

To gain further insight into the magnetic ground state, the electronic structure of $K_2CsYb(PO_4)_2$ was examined via first-principles calculations based on density functional theory. Figure 5(a) presents the calculated band structures and densities of states (DOS) for this compound. Near the Fermi energy, the electronic states are predominantly derived from the $^2F_{7/2}$ multiplet of the Yb $4f$ orbitals, while those located around -1.5 eV arise from the $^2F_{5/2}$ multiplet. The energy separation between these multiplets actually reflects the strong spin-orbit coupling, which splits the f orbitals into lower-energy $^2F_{5/2}$ states and higher-energy $^2F_{7/2}$ states. In an ideal octahedral crystal field, the $^2F_{7/2}$ states would be further split into a Γ_6 doublet, a Γ_7 doublet, and a Γ_8 quartet [52]. However, the trigonal distortion in $K_2CsYb(PO_4)_2$ lowers the local point-group symmetry from the cubic symmetry to D_{3d}, lifting the degeneracy of the Γ_8 quartet and giving rise to two Kramers doublets. Consequently, the four doubly degenerate bands near the Fermi energy are well separated from other states and exhibit minimal dispersion, demonstrating strong f-electron localization, as depicted in Fig. 5(b). Additionally,

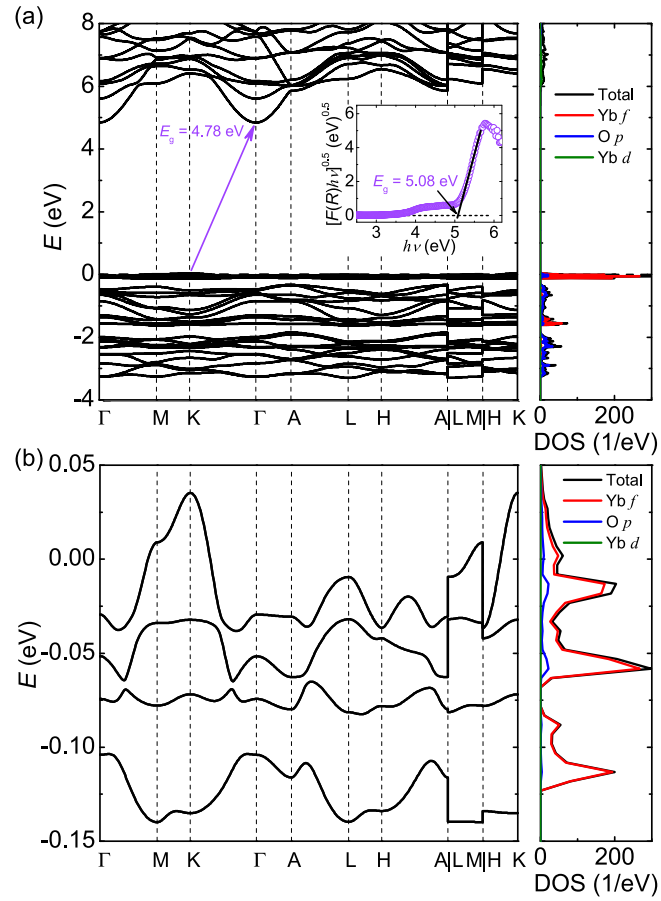


FIG. 5. (a) The calculated band structures and densities of states (DOS) in the ground state of $K_2CsYb(PO_4)_2$. The arrow defines the band gap at high-symmetry points in the reciprocal space. The inset shows the diffusion reflectance spectroscopy of $K_2CsYb(PO_4)_2$ powders measured at room temperature. The solid line denotes a linear fit to the data. (b) Zoom-in view of the isolated manifold of four doubly degenerate bands across the Fermi energy and the associated DOS.

the flat feature of the bands along the Γ-A direction highlights the enhanced two-dimensional nature in this regime, as justified in the crystal structure part. Notably, the isolated doubly degenerate band at the Fermi level implies that the magnetic ground state can be effectively described by a pseudospin $J_{eff} = 1/2$ state, consistent with our specific heat results. It is also worth pointing out that, at the high-symmetry Γ point, the calculated band gap of 4.78 eV corresponds to an electronic transition from the Yb $4f$ to $5d$ states, which is allowed under dipole selection rules. This agrees well with the charge gap of 5.08 eV determined from the optical diffuse reflectance measurements, as shown in the inset of Fig. 5(a). It thus affirms the reliability of our calculation results.

IV. DISCUSSIONS

Ytterbium-based triangular-lattice compounds, particularly $YbMgGaO_4$ and the $AYbCh_2$ family, have emerged as the canonical candidates for realizing the long-sought QSL

state. However, $YbMgGaO_4$ suffers from severe structural disorder that complicates the interpretations of its ground state [14,24–29], while quite a few members of the $AYbCh_2$ family present challenges in growing high-quality single crystals [7,15,37]. In this context, we have successfully prepared the large single crystals of a new disorder-free compound $K_2CsYb(PO_4)_2$. Our band-structure calculations reveal the strong spin-orbit coupling in this regime, similar to that verified in $YbMgGaO_4$ and the $AYbCh_2$ family [4,15]. It is crucial for generating highly anisotropic interactions that enhance quantum fluctuations and thereby favor the stabilization of a QSL state [5,53,54]. While the intralayer Yb-Yb distance in $K_2CsYb(PO_4)_2$ (∼5.6 Å) is larger than in $YbMgGaO_4$ and $AYbCh_2$ (∼3.4 Å) [15,18], leading to weaker magnetic interactions ($J = 0.17$ K), our magnetic susceptibility and specific heat results both point to a spin-disordered ground state, which is a significant signature of QSL behaviors. We fully acknowledge that the extremely weak exchange coupling in this compound may place it in a regime where the spins behave as nearly uncorrelated. In this case, the absence of magnetic order or spin freezing down to 50 mK could indeed be attributed to the paramagnetic response of individual spins. However, we also identify subtle features in our data that may not be fully captured by a simple model of completely noninteracting spins. On one hand, the fit to Schottky anomaly in specific heat has yielded the free-spin fraction of $n \approx 0.5$ at zero field, which rapidly rises to 1 upon applying a small field of 0.5 T, as shown in the inset of Fig. 4(b). This indicates that half of the spins in the ground state remain correlated and they are all excited to higher energy levels by the applied fields, thereby becoming free spins and contributing to the Schottky specific heat; while in a trivial paramagnetic state with noninteracting spins, all of them should be free and thus n will be constant at 1. On the other hand, there is a significant reduction in the effective magnetic moment extracted from the low-temperature Curie-Weiss fit to susceptibility data compared to the high-temperature values. While part of this reduction originates from crystal field effect [49,55], the extent of the suppression is indicative of the development of antiferromagnetic spin correlations, as reported in correlated quantum spin liquid candidates like the $AYbCh_2$ family [37,38]. Thus, our specific heat and magnetic susceptibility data both suggest the correlated spin behaviors in the ground state, despite weak strength of magnetic interactions. Notably, $K_2CsYb(PO_4)_2$ exhibits easy-plane magnetic anisotropy, akin to $AYbCh_2$ [7] but distinct from most reported ytterbium-based triangular-lattice compounds, such as $YbMgGaO_4$ [4,19], $KBaYb(BO_3)_2$ [47,55], $Ba_3Yb(BO_3)_3$ [49,56], and $YbZn_2GaO_5$ [16,57], which show easy-axis behavior. This makes $K_2CsYb(PO_4)_2$ a rare platform for investigating the intriguing physics of easy-plane magnetism. It is reported that geometrically frustrated materials universally exhibit two characteristic energy scales corresponding to two distinguishable peaks in specific heat [58]. For $K_2CsYb(PO_4)_2$, our ultralow-temperature specific heat measurements reveal no peak near the energy scale of magnetic interactions, but only a Schottky anomaly as described in the aforementioned experimental results. We speculate that this Schottky contribution appears to mask the signature of the very weak magnetic interactions, leading to the absence of an expected peak. Given that this peak has been supposededly located at subkelvin temperatures due to the extremely weak magnetic interactions, the putative hidden energy scale would be even lower, likely below our measured temperature of 50 mK. This interpretation is further supported by the substantial residual entropy (∼80% of $R\ln 2$) persisting at 50 mK, indicating the presence of low-energy degrees of freedom that remain inactivated within our measured temperature window. Thus, the compressed energy scales and large residual entropy should align with the physical regime where the lower-energy scale becomes experimentally inaccessible, while the higher scale is suppressed by the dominant Schottky effect. In light of these results, future studies are highly desirable to employ complementary techniques to further identify its ground state. For example, μSR is a powerful tool to confirm the behavior of persistent spin dynamics [21,22], while ultralow-temperature thermal conductivity measurements may reveal mobile gapless excitations characteristic of a QSL [23,27,59]. These investigations will be particularly valuable given the challenge posed by the weak magnetic interactions for inelastic neutron scattering experiments.

Beyond elucidating the ground state of $K_2CsYb(PO_4)_2$, we would like to briefly discuss its potential applications in adiabatic demagnetization refrigeration (ADR). The ADR technique is based on the magnetocaloric effect, which refers to the significant changes of adiabatic temperature of matter in response to the varying external magnetic field [60,61]. A key parameter for coolants is the characteristic temperature T_o, where the specific heat maximum occurs, since this determines the lowest achievable cooling temperature in some sense. Substantial magnetic entropy release near T_o enables efficient heat removal during the demagnetization process. Remarkably, $K_2CsYb(PO_4)_2$ exhibits no specific heat maximum at zero field even down to 50 mK, as shown in Fig. 4. This means its T_o should be located below 50 mK, which is much lower than most of ytterbium-based frustrated magnets reported [48,61,62]. The calculated residual entropy below 50 mK is up to 80% of $R\ln 2$ and is completely released by applying a small field of 0.5 T. The extremely low operating temperatures and field sensitivity position $K_2CsYb(PO_4)_2$ as an outstanding coolant for subkelvin refrigeration.

V. SUMMARY

In summary, we have successfully prepared the high-quality single crystals of a new disorder-free triangular-lattice compound $K_2CsYb(PO_4)_2$, and conducted a comprehensive study of its magnetic properties. The magnetic susceptibility measurements reveal pronounced easy-plane magnetic anisotropy. Remarkably, no magnetic phase transition or spin freezing is observed down to 400 mK. Ultralow-temperature specific heat measurements down to 50 mK confirm the absence of long-range magnetic order and capture a Schottky anomaly, which is well described by a two-level function. Further first-principles calculations suggest a spin-orbit entangled ground state with $J_{\text{eff}} = 1/2$, hinting at the potential exotic physics in this system. Our findings establish $K_2CsYb(PO_4)_2$ as a pristine platform for exploring quantum magnetism free from the influence of disorder.

ACKNOWLEDGMENTS

We gratefully acknowledge Prof. Jian-Xin Li at Nanjing University for providing access to the VASP software package under his group's license and for the use of associated computational resources. We thank Jiawen Zhang for help in processing single-crystal XRD data. This work was supported by the National Key Projects for Research and Development of China under Grants No. 2024YFA1409200 and No. 2021YFA1400400; the Ministry of Science and Technology of China under Grant No. 2022YFA1402702; National Natural Science Foundation of China under Grants No. 12204160, No. 12434005, No. 12225407, No. 12334008, No. 12374148, No. 12204159, No. 12304119, No. 12474113, and No. 52272108; Hubei Provincial Natural Science Foundation of China under Grants No. 2025AFB738 and No. 2023AFA105; Natural Science Foundation of Jiangsu Province under Grant No. BK20233001; and Fundamental Research Funds for the Central Universities.

DATA AVAILABILITY

The data that support the findings of this article are not publicly available. The data are available from the authors upon reasonable request.

[1] J. S. Gardner, Michael J. P. Gingras, and J. E. Greedan, Magnetic pyrochlore oxides, Rev. Mod. Phys. **82**, 53 (2010).

[2] L. Balents, Spin liquids in frustrated magnets, Nature (London) **464**, 199 (2010).

[3] Y. Wang, H. Wu, G. T. McCandless, J. Y. Chan, and M. N. Ali, Quantum states and intertwining phases in kagome materials, Nat. Rev. Phys. **5**, 635 (2023).

[4] Y. Li, G. Chen, W. Tong, L. Pi, J. Liu, Z. Yang, X. Wang, and Q. Zhang, Rare-earth triangular lattice spin liquid: A single-crystal study of $YbMgGaO_4$, Phys. Rev. Lett. **115**, 167203 (2015).

[5] Y.-D. Li, X. Wang, and G. Chen, Anisotropic spin model of strong spin-orbit-coupled triangular antiferromagnets, Phys. Rev. B **94**, 035107 (2016).

[6] Y.-D. Li, Y.-M. Lu, and G. Chen, Spinon Fermi surface $U(1)$ spin liquid in the spin-orbit-coupled triangular-lattice Mott insulator $YbMgGaO_4$, Phys. Rev. B **96**, 054445 (2017).

[7] M. Xie, W. Zhuo, Y. Cai, Z. Zhang, and Q. Zhang, Rare-earth chalcogenides: An inspiring playground for exploring frustrated magnetism, Chin. Phys. Lett. **41**, 117505 (2024).

[8] P. W. Anderson, The resonating valence bond state in La_2CuO_4 and superconductivity, Science **235**, 1196 (1987).

[9] P. A. Lee, N. Nagaosa, and X.-G. Wen, Doping a Mott insulator: Physics of high-temperature superconductivity, Rev. Mod. Phys. **78**, 17 (2006).

[10] A. Yu. Kitaev, Fault-tolerant quantum computation by anyons, Ann. Phys. **303**, 2 (2003).

[11] C. Nayak, S. H. Simon, A. Stern, M. Freedman, and S. Das Sarma, Non-Abelian anyons and topological quantum computation, Rev. Mod. Phys. **80**, 1083 (2008).

[12] P.W. Anderson, Resonating valence bonds: A new kind of insulator? Mater. Res. Bull. **8**, 153 (1973).

[13] Y. Zhou, K. Kanoda, and T.-K. Ng, Quantum spin liquid states, Rev. Mod. Phys. **89**, 025003 (2017).

[14] C. Broholm, R. J. Cava, S. A. Kivelson, D. G. Nocera, M. R. Norman, and T. Senthil, Quantum spin liquids, Science **367**, eaay0668 (2020).

[15] W. Liu, Z. Zhang, J. Ji, Y. Liu, J. Li, X. Wang, H. Lei, G. Chen, and Q. Zhang, Rare-earth chalcogenides: A large family of triangular lattice spin liquid candidates, Chin. Phys. Lett. **35**, 117501 (2018).

[16] R. Bag, S. Xu, N. E. Sherman, L. Yadav, A. I. Kolesnikov, A. A. Podlesnyak, E. S. Choi, I. da Silva, J. E. Moore, and S. Haravifard, Evidence of Dirac quantum spin liquid in $YbZn_2GaO_5$, Phys. Rev. Lett. **133**, 266703 (2024).

[17] Z. Ma, Y. Chen, Z. Fu, S. Li, X.-A. Tong, H. Du, J. P. Embs, S. Zheng, Y. Zhang, M. Liu, R. Zhong, J.-M. Liu, and J. Wen, Magnetically disordered ground state in the triangular-lattice antiferromagnets $Rb_3Yb(VO_4)_2$ and $Cs_3Yb(VO_4)_2$, Phys. Rev. B **111**, 155141 (2025).

[18] Y. Li, H. Liao, Z. Zhang, S. Li, F. Jin, L. Ling, L. Zhang, Y. Zou, L. Pi, Z. Yang, J. Wang, Z. Wu, and Q. Zhang, Gapless quantum spin liquid ground state in the two-dimensional spin-1/2 triangular antiferromagnet $YbMgGaO_4$, Sci. Rep. **5**, 16419 (2015).

[19] Y. Shen, Y.-D. Li, H. Wo, Y. Li, S. Shen, B. Pan, Q. Wang, H. C. Walker, P. Steffens, M. Boehm, Y. Hao, D. L. Quintero-Castro, L. W. Harriger, M. D. Frontzek, L. Hao, S. Meng, Q. Zhang, G. Chen, and J. Zhao, Evidence for a spinon Fermi surface in a triangular-lattice quantum-spin-liquid candidate, Nature (London) **540**, 559 (2016).

[20] J. A. M. Paddison, M. Daum, Z. Dun, G. Ehlers, Y. Liu, M. B. Stone, H. Zhou, and M. Mourigal, Continuous excitations of the triangular-lattice quantum spin liquid $YbMgGaO_4$, Nat. Phys. **13**, 117 (2017).

[21] Y. Li, D. Adroja, P. K. Biswas, P. J. Baker, Q. Zhang, J. Liu, A. A. Tsirlin, P. Gegenwart, and Q. Zhang, Muon Spin Relaxation Evidence for the U(1) Quantum Spin-Liquid Ground State in the Triangular Antiferromagnet $YbMgGaO_4$, Phys. Rev. Lett. **117**, 097201 (2016).

[22] Z. Ding, Z. Zhu, J. Zhang, C. Tan, Y. Yang, D. E. MacLaughlin, and L. Shu, Persistent spin dynamics and absence of spin freezing in the H-T phase diagram of the two-dimensional triangular antiferromagnet $YbMgGaO_4$, Phys. Rev. B **102**, 014428 (2020).

[23] Y. Xu, J. Zhang, Y. S. Li, Y. J. Yu, X. C. Hong, Q. M. Zhang, and S. Y. Li, Absence of magnetic thermal conductivity in the quantum spin-liquid candidate $YbMgGaO_4$, Phys. Rev. Lett. **117**, 267202 (2016).

[24] Z. Ma, J. Wang, Z.-Y. Dong, J. Zhang, S. Li, S.-H. Zheng, Y. Yu, W. Wang, L. Che, K. Ran, *et al.*, Spin-glass ground state in a triangular-lattice compound $YbZnGaO_4$, Phys. Rev. Lett. **120**, 087201 (2018).

[25] Z. Zhu, P. A. Maksimov, S. R. White, and A. L. Chernyshev, Disorder-induced mimicry of a spin liquid in $YbMgGaO_4$, Phys. Rev. Lett. **119**, 157201 (2017).

[26] I. Kimchi, A. Nahum, and T. Senthil, Valence bonds in random quantum magnets: Theory and application to $YbMgGaO_4$, Phys. Rev. X **8**, 031028 (2018).

[27] X. Rao, G. Hussain, Q. Huang, W. J. Chu, N. Li, X. Zhao, Z. Dun, E. S. Choi, T. Asaba, L. Chen, L. Li, X. Y. Yue, N. N. Wang, J. G. Cheng, Y. H. Gao, Y. Shen, J. Zhao, G. Chen, H. D. Zhou, and X. F. Sun, Survival of itinerant excitations and quantum spin state transitions in $YbMgGaO_4$ with chemical disorder, Nat. Commun. **12**, 4949 (2021).

[28] Y. Li, S. Bachus, B. Liu, I. Radelytskyi, A. Bertin, A. Schneidewind, Y. Tokiwa, A. A. Tsirlin, and P. Gegenwart, Rearrangement of uncorrelated valence bonds evidenced by low-energy spin excitations in $YbMgGaO_4$, Phys. Rev. Lett. **122**, 137201 (2019).

[29] J. Wen, S.-L. Yu, S. Li, W. Yu, and J.-X. Li, Experimental identification of quantum spin liquids, npj Quantum Mater. **4**, 12 (2019).

[30] Z. Ma, K. Ran, J. Wang, S. Bao, Z. Cai, S. Li, and J. Wen, Recent progress on magnetic-field studies on quantum-spin-liquid candidates, Chin. Phys. B **27**, 106101 (2018).

[31] T.-H. Han, M. R. Norman, J.-J. Wen, J. A. Rodriguez-Rivera, J. S. Helton, C. Broholm, and Y. S. Lee, Correlated impurities and intrinsic spin-liquid physics in the kagome material herbertsmithite, Phys. Rev. B **94**, 060409(R) (2016).

[32] M. R. Norman, *Colloquium*: Herbertsmithite and the search for the quantum spin liquid, Rev. Mod. Phys. **88**, 041002 (2016).

[33] M. P. Shores, E. A. Nytko, B. M. Bartlett, and D. G. Nocera, A structurally perfect $s = 1/2$ kagomé antiferromagnet, J. Am. Chem. Soc. **127**, 13462 (2005).

[34] J. S. Helton, K. Matan, M. P. Shores, E. A. Nytko, B. M. Bartlett, Y. Yoshida, Y. Takano, A. Suslov, Y. Qiu, J.-H. Chung, D. G. Nocera, and Y. S. Lee, Spin dynamics of the spin-1/2 kagome lattice antiferromagnet $ZnCu_3(OH)_6Cl_2$, Phys. Rev. Lett. **98**, 107204 (2007).

[35] T.-H. Han, J. S. Helton, S. Chu, D. G. Nocera, J. A. Rodriguez-Rivera, C. Broholm, and Y. S. Lee, Fractionalized excitations in the spin-liquid state of a kagome-lattice antiferromagnet, Nature (London) **492**, 406 (2012).

[36] L. Ding, P. Manuel, S. Bachus, F. Grußler, P. Gegenwart, J. Singleton, R. D. Johnson, H. C. Walker, D. T. Adroja, A. D. Hillier, and A. A. Tsirlin, Gapless spin-liquid state in the structurally disorder-free triangular antiferromagnet $NaYbO_2$, Phys. Rev. B **100**, 144432 (2019).

[37] M. M. Bordelon, E. Kenney, C. Liu, T. Hogan, L. Posthuma, M. Kavand, Y. Lyu, M. Sherwin, N. P. Butch, C. Brown, M. J. Graf, L. Balents, and S. D. Wilson, Field-tunable quantum disordered ground state in the triangular lattice antiferromagnet $NaYbO_2$, Nat. Phys. **15**, 1058 (2019).

[38] M. Baenitz, P. Schlender, J. Sichelschmidt, Y. A. Onykiienko, Z. Zangeneh, K. M. Ranjith, R. Sarkar, L. Hozoi, H. C. Walker, J.-C. Orain, H. Yasuoka, J. van den Brink, H. H. Klauss, D. S. Inosov, and T. Doert, $NaYbS_2$: A planar spin-$\frac{1}{2}$ triangular-lattice magnet and putative spin liquid, Phys. Rev. B **98**, 220409(R) (2018).

[39] W. Zhuo, Z. Zhang, M. Xie, A. Zhang, J. Ji, F. Jin, and Q. Zhang, Magnetism of $NaYbS_2$: From finite temperatures to ground state, Sci. China Phys., Mech. Astron. **67**, 107411 (2024).

[40] K. M. Ranjith, S. Luther, T. Reimann, B. Schmidt, P. Schlender, J. Sichelschmidt, H. Yasuoka, A. M. Strydom, Y. Skourski, J. Wosnitza, H. Kühne, T. Doert, and M. Baenitz, Anisotropic field-induced ordering in the triangular-lattice quantum spin liquid $NaYbSe_2$, Phys. Rev. B **100**, 224417 (2019).

[41] P.-L. Dai, G. Zhang, Y. Xie, C. Duan, Y. Gao, Z. Zhu, E. Feng, Z. Tao, C.-L. Huang, H. Cao, *et al.*, Spinon Fermi surface spin liquid in a triangular lattice antiferromagnet $NaYbSe_2$, Phys. Rev. X **11**, 021044 (2021).

[42] G. Kresse and J. Furthmüller, Efficient iterative schemes for *ab initio* total-energy calculations using a plane-wave basis set, Phys. Rev. B **54**, 11169 (1996).

[43] P. E. Blöchl, Projector augmented-wave method, Phys. Rev. B **50**, 17953 (1994).

[44] J. P. Perdew, K. Burke, and M. Ernzerhof, Generalized gradient approximation made simple, Phys. Rev. Lett. **77**, 3865 (1996).

[45] R. Zhong, S. Guo, G. Xu, Z. Xu, and R. J. Cava, Strong quantum fluctuations in a quantum spin liquid candidate with a co-based triangular lattice, Proc. Natl. Acad. Sci. USA **116**, 14505 (2019).

[46] K. M. Ranjith, D. Dmytriieva, S. Khim, J. Sichelschmidt, S. Luther, D. Ehlers, H. Yasuoka, J. Wosnitza, A. A. Tsirlin, H. Kühne, and M. Baenitz, Field-induced instability of the quantum spin liquid ground state in the $J_{\text{eff}} = \frac{1}{2}$ triangular-lattice compound $NaYbO_2$, Phys. Rev. B **99**, 180401(R) (2019).

[47] B. L. Pan, J. M. Ni, L. P. He, Y. J. Yu, Y. Xu, and S. Y. Li, Specific heat and thermal conductivity of the triangular-lattice rare-earth material $KBaYb(BO_3)_2$ at ultralow temperature, Phys. Rev. B **103**, 104412 (2021).

[48] K. Somesh, S. S. Islam, S. Mohanty, G. Simutis, Z. Guguchia, C. Wang, J. Sichelschmidt, M. Baenitz, and R. Nath, Absence of magnetic order and emergence of unconventional fluctuations in the $J_{\text{eff}} = \frac{1}{2}$ triangular-lattice antiferromagnet $YbBO_3$, Phys. Rev. B **107**, 064421 (2023).

[49] R. Bag, M. Ennis, C. Liu, S. E. Dissanayake, Z. Shi, J. Liu, L. Balents, and S. Haravifard, Realization of quantum dipoles in triangular lattice crystal $Ba_3Yb(BO_3)_3$, Phys. Rev. B **104**, L220403 (2021).

[50] J. Khatua, S. Bhattacharya, A. M. Strydom, A. Zorko, J. S. Lord, A. Ozarowski, E. Kermarrec, and P. Khuntia, Magnetic properties and spin dynamics in the spin-orbit driven $J_{\text{eff}} = \frac{1}{2}$ triangular lattice antiferromagnet $Ba_6Yb_2Ti_4O_{17}$, Phys. Rev. B **109**, 024427 (2024).

[51] S. Guo, R. Zhong, K. Górnicka, T. Klimczuk, and R. J. Cava, Crystal growth, structure, and magnetism of the 2D spin 1/2 triangular lattice material $Rb_3Yb(PO_4)_2$, Chem. Mater. **32**, 10670 (2020).

[52] J. G. Rau and Michel J. P. Gingras, Frustration and anisotropic exchange in ytterbium magnets with edge-shared octahedra, Phys. Rev. B **98**, 054408 (2018).

[53] Y.-D. Li, Y. Shen, Y. Li, J. Zhao, and G. Chen, Effect of spin-orbit coupling on the effective-spin correlation in $YbMgGaO_4$, Phys. Rev. B **97**, 125105 (2018).

[54] J. Iaconis, C. Liu, G. B. Halász, and L. Balents, Spin liquid versus spin orbit coupling on the triangular lattice, SciPost Phys. **4**, 003 (2018).

[55] M. B. Sanders, F. A. Cevallos, and R. J. Cava, Magnetism in the $KBaRE(BO_3)_2$ (RE = Sm, Eu, Gd, Tb, Dy, Ho, Er, Tm, Yb, Lu) series: Materials with a triangular rare earth lattice, Mater. Res. Express **4**, 036102 (2017).

[56] C. Y. Jiang, Y. X. Yang, Y. X. Gao, Z. T. Wan, Z. H. Zhu, T. Shiroka, C. S. Chen, Q. Wu, X. Li, J. C. Jiao, K. W. Chen, Y. Bao, Z. M. Tian, and L. Shu, Spin excitations in the quantum dipolar magnet $Yb(BaBO_3)_3$, Phys. Rev. B **106**, 014409 (2022).

[57] Hank C. H. Wu, F. L. Pratt, B. M. Huddart, D. Chatterjee, P. A. Goddard, J. Singleton, D. Prabhakaran, and S. J. Blundell, Spin dynamics in the Dirac U(1) spin liquid $YbZn_2GaO_5$, Phys. Rev. Lett. **135**, 046704 (2025).

[58] P. Popp, A. P. Ramirez, and S. Syzranov, Origin of the hidden energy scale and the f ratio in geometrically frustrated magnets, Phys. Rev. Lett. **134**, 226701 (2025).

[59] M. Yamashita, N. Nakata, Y. Senshu, M. Nagata, H. M. Yamamoto, R. Kato, T. Shibauchi, and Y. Matsuda, Highly mobile gapless excitations in a two-dimensional candidate quantum spin liquid, Science **328**, 1246 (2010).

[60] E. Ambler and R. P. Hudson, Magnetic cooling, Rep. Prog. Phys. **18**, 251 (1955).

[61] D. Jang, T. Gruner, A. Steppke, K. Mitsumoto, C. Geibel, and M. Brando, Large magnetocaloric effect and adiabatic demagnetization refrigeration with $YbPt_2Sn$, Nat. Commun. **6**, 8680 (2015).

[62] A. Liu, J. Zhou, L. Wang, Y. Cao, F. Song, Y. Han, J. Li, W. Tong, Z. Xia, Z. Ouyang, J. Zhao, H. Guo, and Z. Tian, Large magnetocaloric effect in the Shastry-Sutherland lattice compound $Yb_2Be_2GeO_7$ with spin-disordered ground state, Phys. Rev. B **110**, 144445 (2024).